The Plant Cell, Vol. 29: 474–490, March 2017, www.plantcell.org

The Maize MID-COMPLEMENTING ACTIVITY Homolog CELL NUMBER REGULATOR13/NARROW ODD DWARF Coordinates Organ Growth and Tissue Patterning[OPEN]

Marisa Rosa,[a] María Jazmín Abraham-Juárez,[a] Michael W. Lewis,[a] João Pedro Fonseca,[b] Wang Tian,[a] Vicente Ramirez,[a,1] Sheng Luan,[a] Markus Pauly,[a,1] and Sarah Hake[a,c,2]

[a] Department of Plant and Microbial Biology, University of California at Berkeley, Berkeley, California 94720
[b] Department of Biochemistry and Biophysics, University of California San Francisco, San Francisco, California 94143
[c] Plant Gene Expression Center, Agricultural Research Service, U.S. Department of Agriculture, Albany, California 94710

ORCID IDs: 0000-0003-2793-8560 (M.R.); 0000-0002-5468-8176 (M.J.A.-J.); 0000-0001-6953-1529 (S.H.)

Organogenesis occurs through cell division, expansion, and differentiation. How these cellular processes are coordinated remains elusive. The maize (*Zea mays*) leaf provides a robust system to study cellular differentiation due to its distinct tissues and cell types. The *narrow odd dwarf* (*nod*) mutant displays defects at both the cellular and tissue level that increase in severity throughout growth. *nod* mutant leaves have reduced size due to fewer and smaller cells compared with the wild type. The juvenile-to-adult transition is delayed, and proximal distal-patterning is abnormal in this mutant. Differentiation of specialized cells such as those forming stomata and trichomes is incomplete. Analysis of *nod-1* sectors suggests that NOD plays a cell-autonomous function in the leaf. We cloned *nod* positionally and found that it encodes CELL NUMBER REGULATOR13 (CNR13), the maize MID-COMPLEMENTING ACTIVITY homolog. CNR13/NOD is localized to the membrane and is enriched in dividing tissues. Transcriptome analysis of *nod* mutants revealed overrepresentation of cell wall, hormone metabolism, and defense gene categories. We propose that NOD coordinates cell activity in response to intrinsic and extrinsic cues.

INTRODUCTION

Organogenesis results from the activities of cell division, expansion, and differentiation. How these processes are coordinated, and influenced by intrinsic and extrinsic cues, is not fully understood (Sablowski and Carnier Dornelas, 2014; Eichmann and Schäfer, 2015). Leaves provide a useful framework to investigate mechanisms that coordinate individual cell responses with growth and differentiation. Leaves initiate at the flanks of shoot apical meristems (SAMs) and are asymmetric relative to three axes of growth: adaxial-abaxial, medial-lateral, and proximal-distal (Lewis and Hake, 2016). Additionally, developing leaves have a predictable pattern of cell division along a proximal-distal developmental gradient. Maize (*Zea mays*) leaves are especially useful for studying patterning. These leaves are composed of a proximal sheath that grips the stem, a distal blade, and a junction region of the auricle and ligule. The auricle serves as a hinge, allowing the blade to tilt back, while the ligule acts as a gasket. Although the ligule itself is mostly derived from adaxial epidermis, vasculature coalesces at that region (Becraft et al., 1990) and abaxial layers become rigid (Sun et al., 2015). Thus, numerous levels of cell and tissue coordination are evident in order to form a mature maize leaf.

The *CELL NUMBER REGULATOR* (*CNR*) gene family was identified in maize through homology with a tomato (*Solanum lycopersicum*) quantitative trait locus, fw2.2, which influences fruit size up to 30% (Guo et al., 2010; Frary et al., 2000). Similar to FW2.2, CNR1 and CNR2 expression levels have an inverse impact on cell number, although cell size remained unchanged. These are plant-specific, membrane-localized cysteine-rich proteins that carry a PLAC8 domain (named after a family of human placenta-specific proteins of unknown function) (Libault and Stacey, 2010). PLAC8-containing proteins were also identified in *Arabidopsis thaliana*. Overall, these proteins are membrane localized and may function in metal transport (Song et al., 2004, 2010; Nakagawa et al., 2007; Yamanaka et al., 2010). Among them are the MCAs (MID-COMPLEMENTING ACTIVITY), which are thought to be involved in Ca^{2+} uptake. MCAs have a conserved structure, with a PLAC8 domain in the C terminus and a mid-portion coiled-coil domain. The N terminus diverges from other PLAC8-containing proteins by having sequence homology to the regulatory region of various rice (*Oryza sativa*) protein kinases and a EF-hand-like motif known to interact with Ca^{2+} (Iida et al., 2013). In most eudicots, two MCA-coding genes are present, a likely result of separate duplication events, while monocots have only one of these genes (Kurusu et al., 2013).

The Arabidopsis MCA1 was identified by its ability to complement the low Ca^{2+} and related lethality phenotypes of *mid1* (*mating induced death1*) yeast mutants upon mating induction (Iida et al., 1994; Fischer et al., 1997; Nakagawa et al., 2007; Yamanaka et al., 2010; Kurusu et al., 2012a, 2012c). Mid is

[1] Current address: Institute for Plant Cell Biology and Biotechnology, Heinrich-Heine University, 40225 Düsseldorf, Germany.
[2] Address correspondence to hake@berkeley.edu.
The author responsible for distribution of materials integral to the findings presented in this article in accordance with the policy described in the Instructions for Authors (www.plantcell.org) is: Sarah Hake (hake@berkeley.edu).
[OPEN]Articles can be viewed without a subscription.
www.plantcell.org/cgi/doi/10.1105/tpc.16.00878

a putative regulatory subunit of a high-affinity, low-capacity Ca^{2+} influx system that has Cch1 as the putative pore-forming subunit (Iida et al., 1994; Fischer et al., 1997; Muller et al., 2001; Rigamonti et al., 2015). Interestingly, *cch1* lethality was also partially complemented by MCA expression (Yamanaka et al., 2010; Kurusu et al., 2012a, 2012c). Experiments in various cell types showed that overexpression of MCAs leads to increased Ca^{2+} uptake under normal and membrane-distorting conditions (Nakano et al., 2011; Kurusu et al., 2012a, 2012b, 2012c; Furuichi et al., 2012). Furthermore, as Mid is thought to have stretch-activated Ca^{2+} uptake functions and MCA1 is required for mechanoperception in roots, it was suggested that MCAs are stretch-activated Ca^{2+} channels (Nakagawa et al., 2007).

Here, we describe the *narrow odd dwarf* (*nod*) mutant, which has pleiotropic phenotypes that affect vegetative and reproductive development in maize. *nod* encodes CNR13, the maize homolog of MCA proteins. *nod-1* has an overall reduction in size and organ patterning defects. These severe phenotypes derive from defects in cell division, expansion, and differentiation. Analysis of *nod-1* mosaic plants suggested that CNR13/NOD has a cell-autonomous function. Transcriptomic analysis revealed that multiple genetic pathways contribute to the pleiotropy of the *nod* phenotype, including leaf patterning factors and gibberellin biosynthesis. Interestingly, *nod* mutants also appear to have a constitutive upregulation of pathogen response pathways. Therefore, we propose that CN13/NOD functions to coordinate growth and patterning in response to developmental (intrinsic) and environmental (extrinsic) cues.

RESULTS

nod Mutants Have Smaller Organs Due to Fewer and Smaller Cells

The recessive *nod-1* mutant was discovered in an EMS F2 population, with mutagenized B73 pollen crossed onto A619 female flowers. Mutants were crossed into B73 four generations prior to phenotypic analysis. *nod-1* plants have pleiotropic phenotypes in both vegetative and reproductive development (Figure 1). The mutants are notably smaller than the wild type as early as 2 weeks after sowing (Figure 1A). This size difference is exacerbated at maturity and clearly affects leaf dimensions, plant height, and stem diameter (Figures 1B to 1F and 1J). A loss of apical dominance adds to a striking change in plant architecture, giving mutant plants a dwarf, bushy appearance due to derepression of axillary bud growth (Figures 1C and 1J). The main shoot in *nod-1* has extremely abridged internode elongation, fewer internodes (only 6% of wild-type stem height) and asymmetrical shape (Figures 1D and 1J). Leaves are reduced in length, width, and number (Figures 1F and 1J) and have irregular surfaces and chlorotic patches (Figure 1F). These phenotypes are obvious from the first leaves and become progressively more severe (Figure 1F; see below). *nod-1* tassels are barren and necrotic (Figures 1G to 1H), although small, partially fertile ears are produced on the main shoot and tillers (Figure 1I).

Leaf defects, increased tiller outgrowth, and abnormal tassel production suggested a SAM defect. Analysis of longitudinal sections revealed that 3-week-old *nod-1* meristems are proportionally smaller than the wild type but have a normal shape (Figures 2A and 2B). Additionally, the meristem marker KNOTTED1 (KN1) localized to the SAM and was excluded from leaf primordia, similar to the wild type (Figure 2C), suggesting normal meristem identity. Sections of 5-week-old apices showed a transitioning SAM in both wild-type and *nod-1* plants (Figure 2D). Later, the inflorescence meristem fails to initiate lateral primordia and differentiates (Figures 2E to 2G, arrows). Tassel elongation is reduced and few spikelet pairs are produced, sometimes appearing, instead, singly or in triplicate (Figures 2H to 2J). This suggests tassels initiate but don't progress.

We asked if the *nod-1* size reduction was caused by a decrease in cell number due to cell proliferation defects or by reduced cell expansion. Mutant leaf cells looked smaller and in fewer layers than in the wild type (Supplemental Figures 1A to 1D). Mutant interstomatal epidermal cells in leaf 4 were uniformly smaller than the wild type in width, length, and thickness (82, 84 and 73% of the wild type) (Supplemental Figures 1E to 1G). The blade length of leaf 4 is 44% of the wild type (Figure 1J), while cell size is only reduced to 84%, suggesting a reduction in cell number as well. Furthermore, from the measurements, we extrapolated the average cell area and volume in *nod-1* to be 70 and 50% of the wild type, respectively (Supplemental Figure 1H), which is not enough to explain the strong reduction in overall plant size. Therefore, *nod-1* mutants are defective in both cell proliferation and expansion.

A second allele, *nod-2*, was identified in an EMS population in the A619 inbred background. This mutant failed to complement *nod-1.* Both alleles have similar phenotypes when compared in the same inbred background (Supplemental Figure 2). Interestingly, the severity of the *nod* mutant phenotypes varies with the genetic background (Supplemental Figure 2). We focused our analysis on B73, which produces the most severe phenotype, in hopes of discovering the connection between the many pleiotropic traits.

nod Mutants Have Proximal Distal Patterning Defects

In normal maize leaves, the proximal sheath and distal blade are separated by a clear border where the fringe-like ligule and hinge-forming auricle reside (Figure 3A). The preligule band is visible early in leaf primordia as a line of cells that divide transversely, longitudinally, and eventually, outward to initiate the ligule (Sylvester et al., 1990). *nod-1* has a gradual disruption in proximal-distal leaf patterning; both auricle and ligule tissues are reduced in the first leaves produced but are absent in later leaves (Figures 3A to 3E; Supplemental Figures 3A and 3B). If produced, the ligule is restricted to leaf margins and is replaced at the midrib by a mass of unorganized cells forming outgrowths (Figure 3E, open arrow). Both phenotypes are obvious, even in young developing leaves (Supplemental Figure 3G). Divisions at the preligule also appear in a more vertical pattern in *nod-1* than in the wild type (Supplemental Figure 3G). Additionally, the left and right halves of the mutant leaves are asymmetric and have abnormal cell proliferation at both the adaxial and abaxial surfaces (Figures 3F to 3H; Supplemental Figure 3C). The sheath is also abnormal in *nod-1* (Supplemental Figures 3D to 3F), indicating that leaf-patterning defects are not restricted to the sheath-blade border. When grown in the greenhouse during winter, mutant seedlings accumulated high

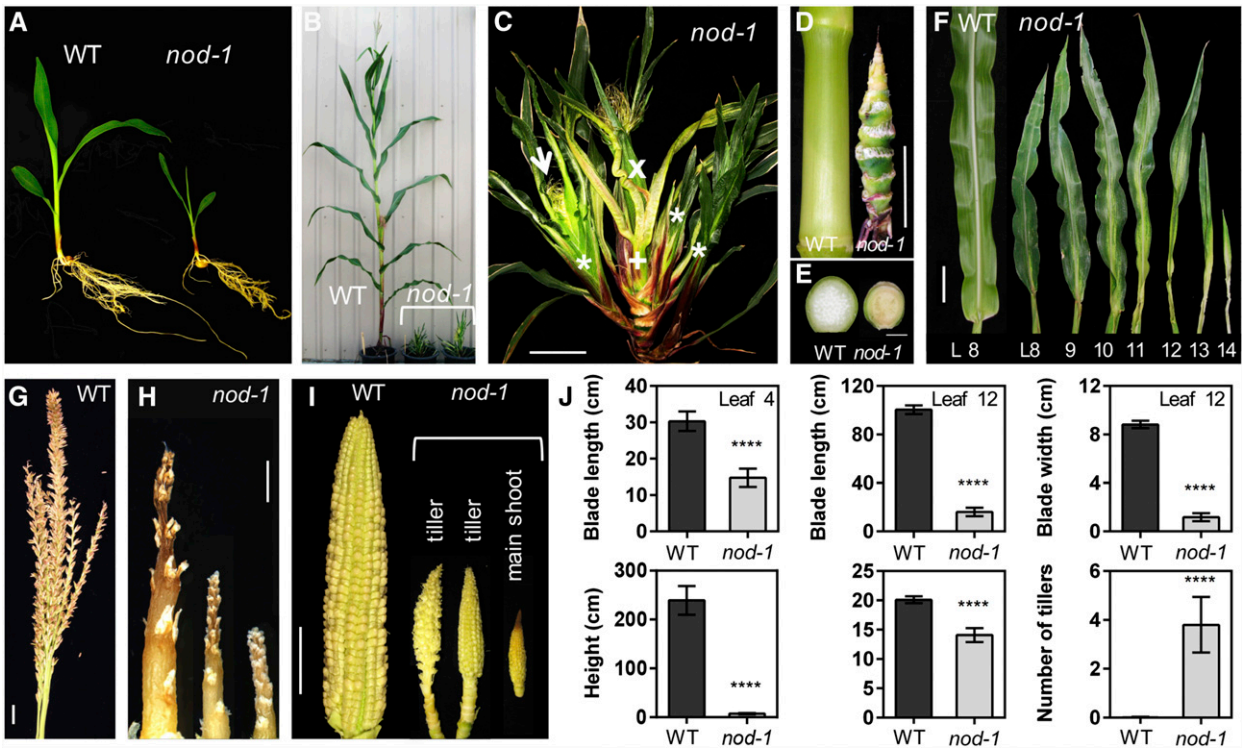

Figure 1. *nod* Mutants Have Pleiotropic Developmental Phenotypes.

(A) Two-week-old wild-type and *nod-1* plants.
(B) Mature wild-type and *nod-1* plants.
(C) Detail of *nod-1* plant. (+), main shoot; (*), tillers; (X), ear. Arrow, ear in tiller. Bar = 4 cm.
(D) Wild-type and *nod-1* mature stems. Bar = 4 cm.
(E) Cross section of mature wild-type and *nod-1* stems. Bar = 1 cm.
(F) Wild-type leaf 8 and *nod-1* leaves 8 to 14. Leaf 1 is the first produced by the plant. Bar = 4 cm.
(G) Wild-type male inflorescence. Bar = 2 cm.
(H) Detail of *nod-1* male inflorescences. Bar = 1 mm.
(I) Wild-type and *nod-1* unfertilized ears. Bar = 4 cm.
(J) Measurement of wild-type and *nod-1* phenotypes.
Data represent mean ± SD. $n = 10$ plants. ****$P \leq 0.0001$; unpaired two-sample Student's t tests.

levels of pigment in the sheath (Figures 3B to 3D). This pigmentation was sometimes present in wild-type plants, although with less intensity.

To further investigate the ligule patterning defects in *nod-1*, we performed immunolocalization using an antibody to the LIGULELESS1 (LG1) protein, which is required for developmental patterning of the blade-sheath boundary (Moreno et al., 1997). LG1 accumulates at the preligule region in leaf primordia (Lewis et al., 2014) and activates various leaf patterning genes (Johnston et al., 2014). Surprisingly, LG1 accumulation is normal in *nod-1*, even at the midrib (Figures 3I and 3J). Thus, the signal for ligule initiation and growth is present, but the cell divisions and differentiation downstream of ligule signaling are abnormal.

nod-1 Has Multiple Defects in Cell Differentiation

Given the increasing severity of *nod-1* during development, we examined the phenotypes of juvenile and adult leaf blades. Normal juvenile leaves are small, have simple cell walls, and lack adult specialized cell types (e.g., hairs and bulliform cells) (Figures 4A and 4B) (Dudley and Poethig, 1993; Sylvester et al., 1990). In the wild type, the first four leaves are fully juvenile, five to seven have mixed identities, and the rest are adult. In *nod-1* mutants, leaf 8 is still juvenile, as confirmed by purple TBO staining to indicate juvenile waxes (Dudley and Poethig, 1993), and it lacks hairs (Figure 4B). Leaf 10 and later exhibit adult traits, including the presence of hairs and cell wall crenulation (Sylvester et al., 1990), indicating that the juvenile-to-adult transition is delayed in *nod-1*.

The patterning defects of *nod-1* expand beyond the sheath-blade boundary. Patches of cells with high wall autofluorescence are present in the proximal blade and close to the midrib in *nod-1* (Figures 4D and 4E), coinciding with a lack of chlorophyll (Figure 4A, region b). These regions are unorganized and composed of abnormal, small cells (Figures 4F and 4G, *nod-1 b*) that often proliferate, replacing normal epidermal, mesophyll (Figure 4D), and hypodermal sclerenchyma that top vascular bundles (Figures

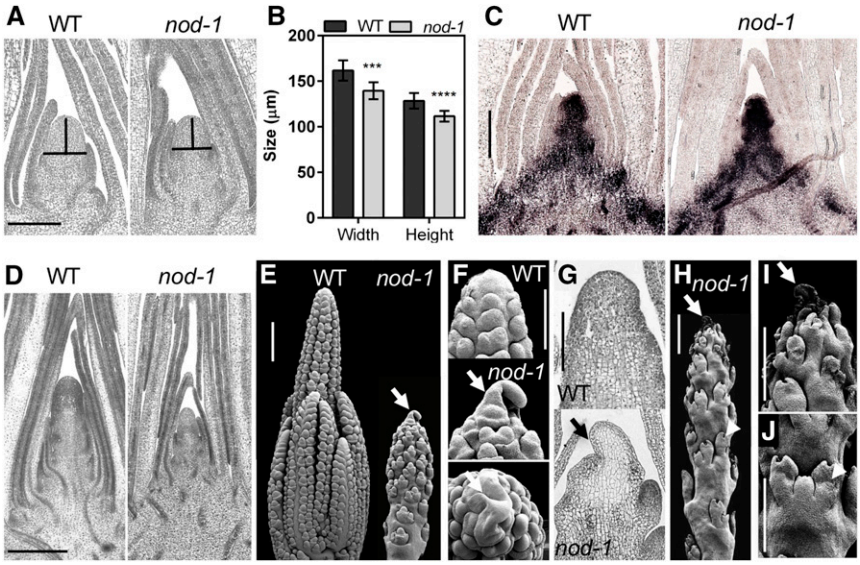

Figure 2. Analysis of *nod-1* Shoot Apical and Inflorescence Meristems.

(A) Wild-type and *nod-1* TBO-stained longitudinal sections of 3-week-old SAMs. Bar = 200 μm.
(B) SAM size (height and width) of 3-week-old wild-type and *nod-1* plants. Data represent mean ± SD. $n = 10$ SAMs. ***$P \leq 0.001$; ****$P \leq 0.0001$; unpaired two-sample Student's *t* tests.
(C) KN1 immunolocalization of 3-week-old wild-type and *nod-1* apices. Bar = 200 μm.
(D) Wild-type and *nod-1* TBO stained longitudinal sections of 5-week-old apices. Bar = 500 μm.
(E) Scanning electron micrograph of wild-type and *nod-1* developing male inflorescence. Bar = 1 mm.
(F) Detail of inflorescence meristem of developing tassels in **(E)**. The wild type is shown from the side. *nod-1* is shown from the side and from above. Bar = 500 μm.
(G) Wild-type and *nod-1* longitudinal sections of developing male inflorescence. Bar = 500 μm.
(H) Scanning electron micrograph of *nod-1* male inflorescence. Bar = 1 mm.
(I) Detail of inflorescence in **(H)**. Bar = 500 μm.
(J) Detail of a spikelet triplicate present in a male inflorescence. Bar = 500 μm.
Arrow, differentiated inflorescence meristem; triangle, odd numbered spikelets.

4C to 4E, arrows). This change in cell identity can by visualized in transverse leaf sections by the lack of phloroglucinol staining (Supplemental Figures 4A and 4B, arrows). The staining pattern difference is also apparent in stem cross sections (Supplemental Figure 4C) and suggests a change in lignin content and/or composition.

Other obvious defects in cell differentiation involve hairs and stomates. The specialized cells at the base of macrohairs are reduced or missing in *nod-1*, and rows of ectopic and enlarged prickle hairs appear above the veins (Figure 4F, triangle) and, randomly, in the abaxial surface (Figure 4G). In monocots, stomata complexes, comprising two subsidiary cells flanking two guard cells, arise from a sequence of three cell divisions followed by cell differentiation (Facette and Smith, 2012). *nod-1* blades have multiple types of abnormal stomata (Supplemental Figures 1D and 5A, triangle). The presence of stomata with altered cell number (divisions) and abnormal shape (differentiation) (Supplemental Figure 5B) indicates defects in all patterning steps. The severity increases close to the midrib, in the proximal blade region, and in the abaxial surface (Supplemental Figure 5B), recapitulating other cell organization and patterning defects (Figure 4). Stomata density is also reduced in *nod-1* mutant leaves (Supplemental Figure 5C).

Taken together, these data suggest that NOD is required for normal cell division, expansion, and differentiation. The failure of these basic cellular processes in the mutant leads to pleiotropic consequences that affect multiple aspects of plant development in maize.

NOD Is a MCA Protein

We mapped *nod-1* to an interval of 244 kb containing four gene models, with 50 recombinants detected among 700 individuals. After sequencing, we found a change of C to T in one of the four predicted genes, GRMZM2G027821. This mutation was localized in the second exon of the gene and caused a conversion from a glutamine (Q) to a stop codon (Figure 5A). The second allele, *nod-2*, has a missense mutation of C to T that converted a highly conserved proline (P) to a leucine (L) (Supplemental Figure 6A). A long (T01) and a short (T02) transcript are produced from this locus (Figure 5A), but *nod*_T02 levels are much lower than *nod1*_T01 levels (Figure 5B). The levels of both transcripts are reduced to approximately one-third of the wild type in *nod-1* and are unchanged in *nod-2* (Figure 5B). To study protein abundance, we raised an antibody against NOD and used it for protein gel blot analysis. The antibody detected a specific 48-kD

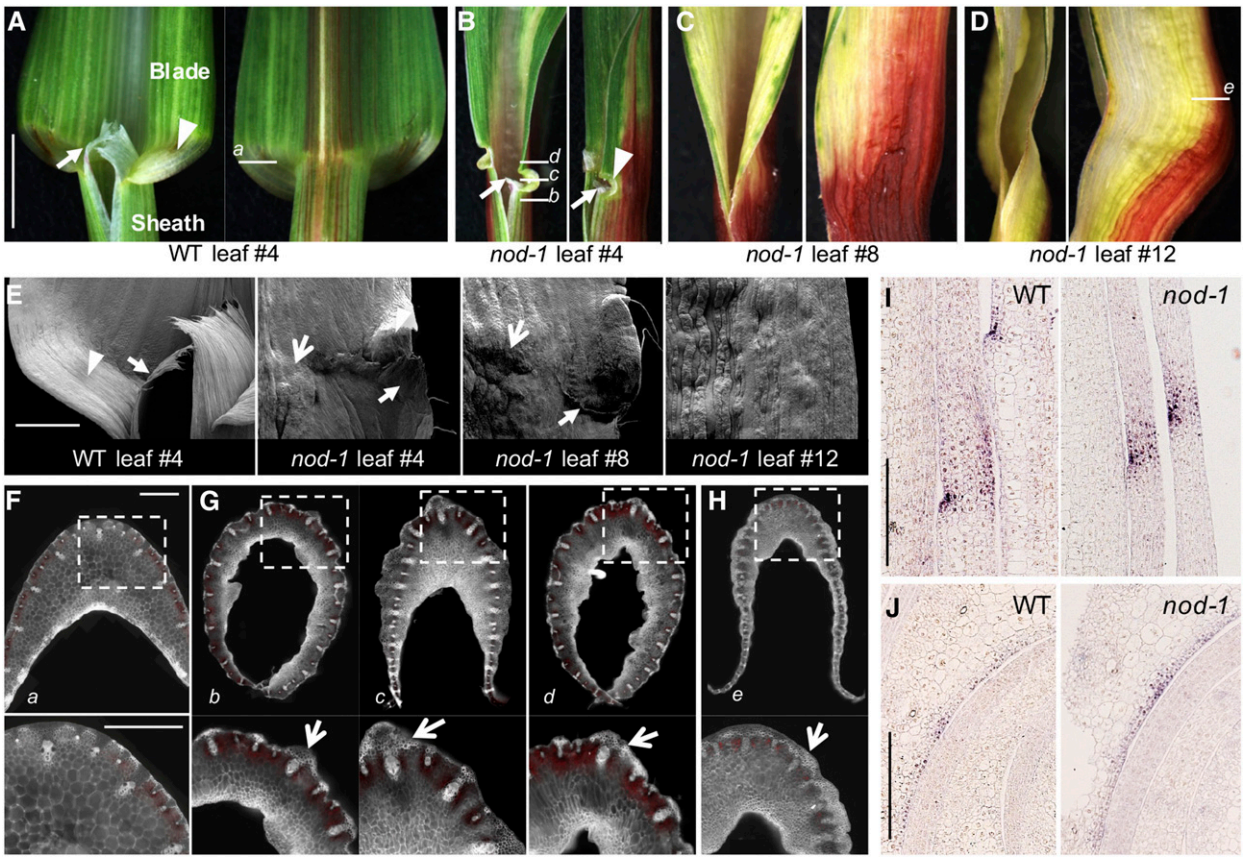

Figure 3. *nod-1* Leaves Have Proximal-Distal Patterning Defects.

(A) to **(D)** Light photographs of wild-type and *nod-1* leaves.
(A) Adaxial (left) and abaxial (right) sides of wild-type leaf 4.
(B) to **(D)** Adaxial (left) and side (right) view of *nod-1* leaf 4 **(B)**, 8 **(C)**, and 12 **(D)**. Bar = 5 mm.
(E) Scanning electron micrograph of adaxial blade-sheath border region in wild-type leaf 4 and *nod-1* leaves 4, 8, and 12. Bar = 1 mm.
(F) to **(H)** Hand sections of wild-type **(F)** and *nod-1* (G-H) blade-sheath borders. Leaf sections are oriented with the abaxial surface to the top. Bottom panel is a detail of boxed region in the top panel. Gray, cell wall autofluorescence; red, chlorophyll autofluorescence. Bar = 200 μm.
(F) Section through wild-type region *a* in **(A)**.
(G) Section through *nod-1* regions *b* (left panel), *c* (middle panel), and *d* (right panel) shown in **(B)**.
(H) Section of *nod-1* through region *e* in **(D)**.
(I) and **(J)** Immunolocalization of LG1 in the wild type and *nod-1*. Longitudinal **(I)** and transverse sections **(J)**. Bar = 200 μm.
Arrow, ligule; triangle, auricle; open arrow, unorganized outgrowths.

protein in shoot apices, consistent with the prediction of a 421-amino acid protein produced by *nod*_T01 (Figure 5C). The corresponding band was absent in *nod-1* and reduced in *nod-2*. No other bands corresponding to a putative shorter protein were detected in *nod-1*, suggesting that it is a protein null allele (Figure 5D). No band corresponding to *nod*_T02 was observed in the analyzed samples.

nod encodes the maize MCA protein, a PLAC8-containing protein previously annotated as CNR13 (Guo et al., 2010). NOD maintains the key features of other MCAs, including putative transmembrane regions in both N- and C-terminal regions, and a coil-coiled structural domain (Figure 5D; Supplemental Figure 6A). Previous work with Arabidopsis and rice MCA proteins indicated the presence of an EF-hand-like motif, a region often found in rice kinases named ARPK in the N-terminal half of the proteins, and a STYcK region (Nakagawa et al., 2007; Liu et al., 2015), which appear conserved in NOD (Supplemental Figure 6A). Analysis by RNA-seq indicated that *nod* is expressed throughout maize plants, with higher levels in developing organs (Supplemental Figure 6C) (Stelpflug et al., 2016). To analyze protein subcellular localization, we expressed Pro35S:NOD:YFP constructs transiently in wild tobacco (*Nicotiana benthamiana*). YFP signal was apparent at the plasma membrane of epidermal cells (Figure 5E), confirming previous MCA localization data (Nakagawa et al., 2007; Yamanaka et al., 2010; Kurusu et al., 2012a, 2012c). We used the NOD antibody to study protein localization in sections of wild-type and *nod-1* shoot apices but were unable to identify any signal.

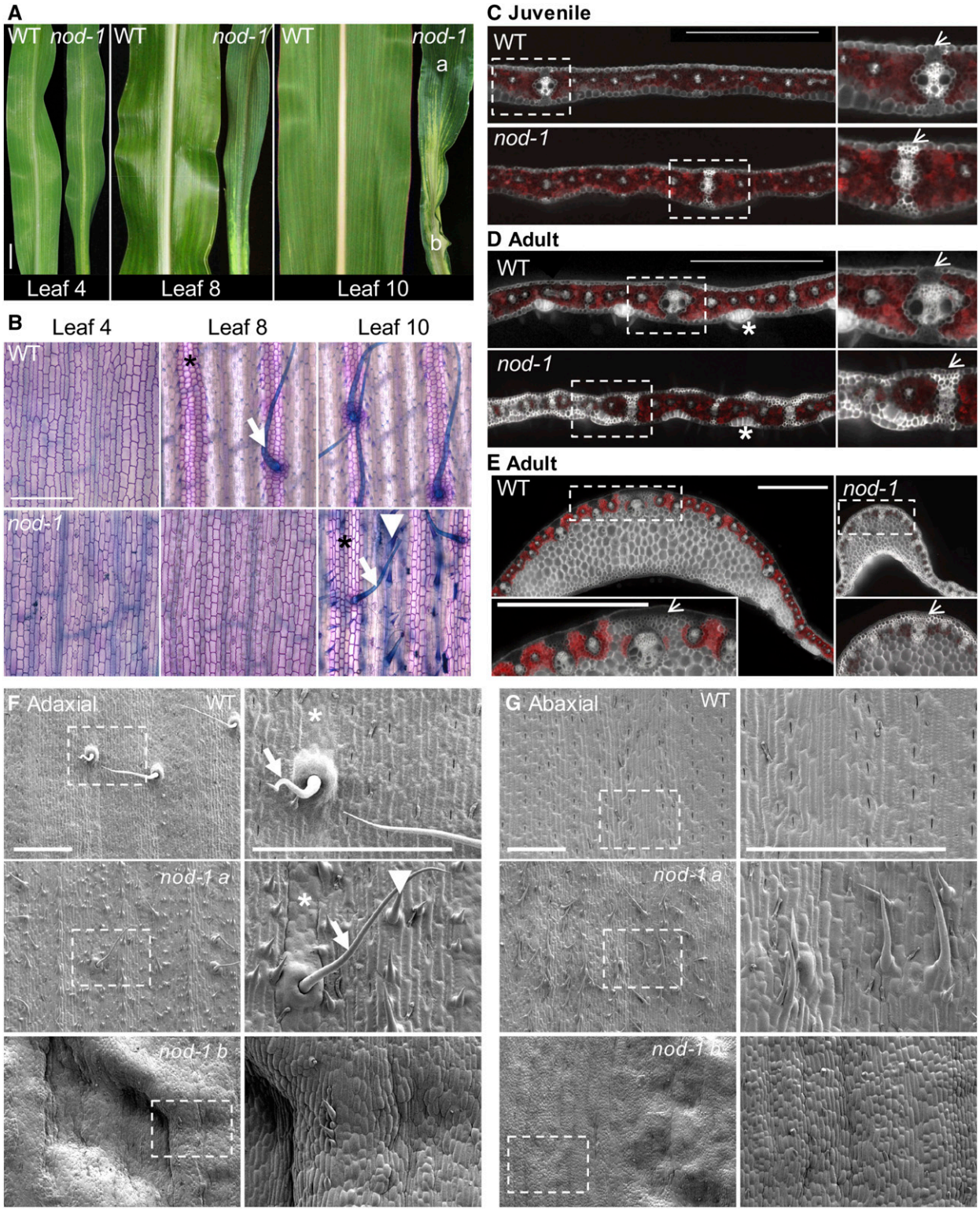

Figure 4. *nod-1* Mutant Leaves Have Defects in Patterning of Cell Differentiation.

(A) Detail of wild-type and *nod-1* mid-portions of leaf 4, 8, and 10 blades. a, distal leaf blade; b, proximal leaf blade. Bar = 1 cm.
(B) Cleared and TBO stained wild-type and *nod-1* blades of leaf numbers 4, 8, and 10.

Given the ability of MCA to partially complement *mid1* yeast mutants and increase Ca^{2+} uptake (Nakagawa et al., 2007; Yamanaka et al., 2010; Kurusu et al., 2012c), we investigated whether NOD is able to rescue the lethality of the Ca^{2+}-deficient *mid1* yeast mutants upon treatment with the α-factor. Three hours after treatment, the lethality of *mid1* increased to 31%, an effect completely rescued by transformation with MID1 (Figure 5F). Expression of NOD partially rescued the *mid1* phenotype (18% lethality), whereas the protein encoded by *nod-2* (NOD-2) provided no rescue. Previous work has explored the possibility that MCAs form plasma membrane-localized mechanosensing Ca^{2+} channels. Although Furuichi et al. (2012) reported some channel activity, we were unable to confirm their findings in experiments with *Xenopus laevis* oocytes under our experimental conditions (Supplemental Figure 6D). Taken together, our results show that the *mid1*-complementing activity of MCAs is conserved in NOD, but obtaining a complete understanding of the molecular activity of NOD requires further study.

NOD Functions Cell Autonomously

We performed a mosaic analysis (Becraft et al., 1990; Foster et al., 2004) to determine the autonomy of the *nod-1* phenotype and to further characterize the function of NOD. Cell-autonomous gene products only affect the phenotype of the cells where they are expressed, while non-cell-autonomous gene products are able to rescue adjacent mutant cells (Candela and Hake, 2008). *nod-1* was marked with the linked albino mutant marker *viviparous5* (*vp5*) (Becraft et al., 2002) (see Methods). The mixed genetic background (B73/Hi17) produced milder mutant phenotypes then B73, but *nod-1* phenotypes were clearly expressed in homozygous *vp5* seedlings (Figures 6A and 6B). X-ray-induced loss of the top of chromosome 1 (Figure 6C) created albino (*nod-1*/− *vp5*/− hemizygous) sectors on normal (heterozygous) green leaves (Figures 6D to 6F).

The sector depicted in Figure 6 extends along the entire length of the leaf, occupies 3% of the leaf blade width, and is white in all cell layers. It is flanked by narrow pale-green regions, in which only the L1 and L2 layers are albino (Figure 6D). The mutant sector interrupted and reduced the size of the ligule (Figure 6E, arrow) and displayed multiple *nod-1* phenotypes, including smaller vascular bundles, irregular leaf surface, and ectopic hairs (Figures 6G to 6J). Those phenotypes are absent in the green tissue of mosaic leaves or in *vp5*/− sectors of *nod-1*/+ plants (Figures 6J to 6M). Additional *nod-1* defects seen in the sector include abnormal stomata development, misshapen cells, and reduced cell width (Figure 6N). The cell width was reduced in all *nod-1* albino tissues and even at the borders, when only the abaxial L1 and L2 are mutant (Figure 6O), suggesting that the presence of wild-type internal mesophyll cells is not enough to recover the mutant phenotype. The same phenotypes were observed in other sectors with similar composition (Figure 6P). While we cannot exclude the possibility that NOD may influence the phenotype of directly adjacent cells through a short-distance signal, at the tissue level, wild-type cells are not able to rescue mutant traits, suggesting a cell-autonomous function for NOD.

nod-1 Changes Transcription of Multiple Pathways

To address the pleiotropic effects of *nod* mutants, we performed expression profiling by RNA-seq using 3-week-old plants (Supplemental Figures 7A to 7C and Supplemental Data Set 1). Using a false discovery rate (FDR) of <0.05, 9533 of a total of 25,038 genes were deemed differentially expressed (DE) between the wild type and *nod-1* (Supplemental Data Set 2). To focus on the most significant genes, we used a stringent criterion of FDR < 0.01 and fold change > 2, which led to 4137 DE genes. Of those, 3028 and 1109 were up- and downregulated, respectively. The *nod* transcript levels are reduced to approximately one-third of the wild type, consistent with the RT-qPCR analysis (Figure 5B; Supplemental Data Set 2).

To investigate proximal-distal leaf patterning, we analyzed the overlap of *nod-1* DE and genes enriched at different regions of the leaf primordia (blade, sheath, and ligule) (Johnston et al., 2014). Overrepresentation of all categories is found in both up- and downregulated *nod-1* genes (Supplemental Data Set 3), indicating a global misregulation of leaf patterning factors. A significant overlap is also found between *nod-1* and genes both up- and downregulated in *lg1* (Johnston et al., 2014). As the expression of *lg1* remains unchanged (Figures 3I and 3J; Supplemental Data Set 2), the data support the idea that LG1 signal fails to transmit correctly in *nod-1*. KNOX genes (such as *kn1*) and their targets have a proposed role in proximal-distal leaf patterning (Bolduc et al., 2012a; Johnston et al., 2014). Comparison of *nod-1* DE genes with those changed in *kn1* mutants or bound by KN1 (Bolduc et al., 2012b) shows a statistically significant enrichment, particularly in the *nod-1* downregulated group. These changes in gene expression are likely related to the proximal-distal patterning defects observed in *nod-1* mutants.

To identify additional cellular pathways or processes changed in *nod-1*, we tested the enrichment of MapMan categories (Thimm et al., 2004). We found several overrepresented ($P < 0.01$) functional categories that correlated well with the *nod-1* phenotype (Figure 7A). The expression of SBP transcription factors, which function in vegetative phase change in maize (Chuck et al., 2007;

Figure 4. (continued).

(C) to **(E)** Hand sections of wild-type and *nod-1* mid-blade region on juvenile **(C)** and adult blades **(D)** and adult midrib **(E)**. Leaf sections are oriented with the abaxial surface to the top. Right or bottom panel, close-up of boxed region. Bar = 1 mm.

(F) and **(G)** Scanning electron micrograph of adaxial **(F)** and abaxial **(G)** wild-type and *nod-1* adult blades. *a* and *b* correspond to regions in **(A)**. Right panel, close-up of boxed region. Bar = 500 μm.

Asterisk, rows of bulliform cells; arrow, macrohair; triangle, ectopic hairs; open arrow, regions of hypodermal sclerenchyma.

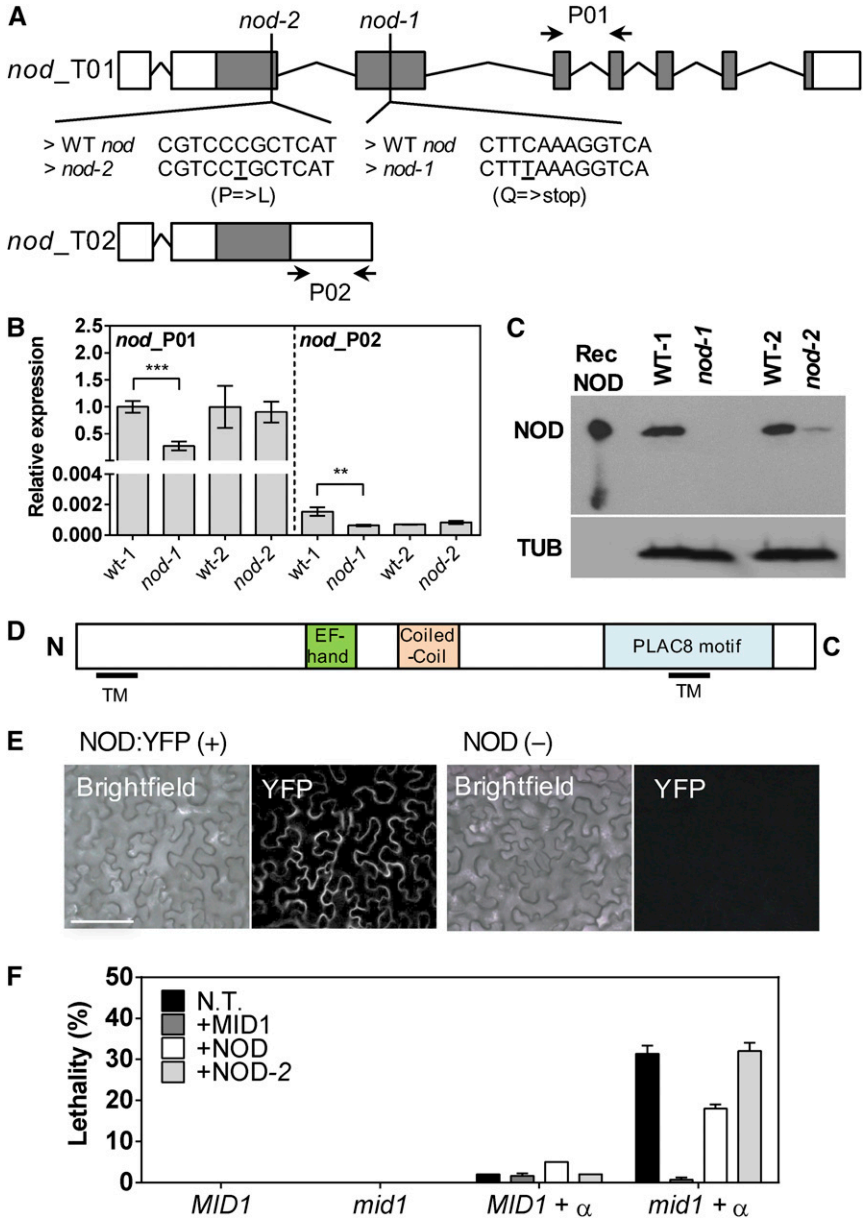

Figure 5. NOD Is a MCA Family Protein.

(A) Structure of the *nod* gene. Two transcripts (T01 and T02) are produced. *nod-1* and *nod-2* mark the location the mutations. Gray boxes, exons; lines, introns; clear boxes, untranslated regions. P01 and P02, primer pairs used for T01 and T02.

(B) Quantitative RT-PCR analysis of *nod* T01 and T02 in vegetative shoot apices. Results shown are relative to the *gapdh* gene. Data represent mean ± SD. $n = 3$ shoots. ***P ≤ 0.001; **P ≤ 0.01; unpaired two-sample Student's *t* tests.

(C) Protein gel blot analysis of NOD protein levels in wild-type and *nod* mutant vegetative shoot apices. TUB, TUBULIN used as a control.

(D) Structure of MCA proteins showing predicted domains. Black bars, potential transmembrane segments (TM).

(E) Transient expression of *nod* in wild tobacco cells. Expression of NOD:YFP and NOD (negative control) driven by the constitutive 35 promoter. Bright-field and YFP channel images of the same region are presented. Bar = 200 μm.

(F) Cell viability of MID1 and *mid1* mutant yeast with or without treatment with the α-factor (α). Cells were not transformed (N.T.) or transformed with MID1, NOD, and NOD-2 (mutant version encoded by *nod-2*). Data represent mean ± SD. $n = 3$ (10,000 cells each). ***P ≤ 0.001; ****P ≤ 0.0001; χ^2 test.

Wu and Poethig, 2006), is reduced in *nod-1*, confirming the phenotypic analysis (Figure 4B). Accordingly, *gl1*, a marker of juvenility, is strongly overexpressed in this mutant (Supplemental Data Set 2). To determine how much of the overall transcriptional changes could be a result of this delay in phase transition, we compared the *nod-1* data set with juvenile or adult-specific genes in developing leaves (Beydler et al., 2016). As expected, juvenile and adult-specific genes were overrepresented in *nod-1*

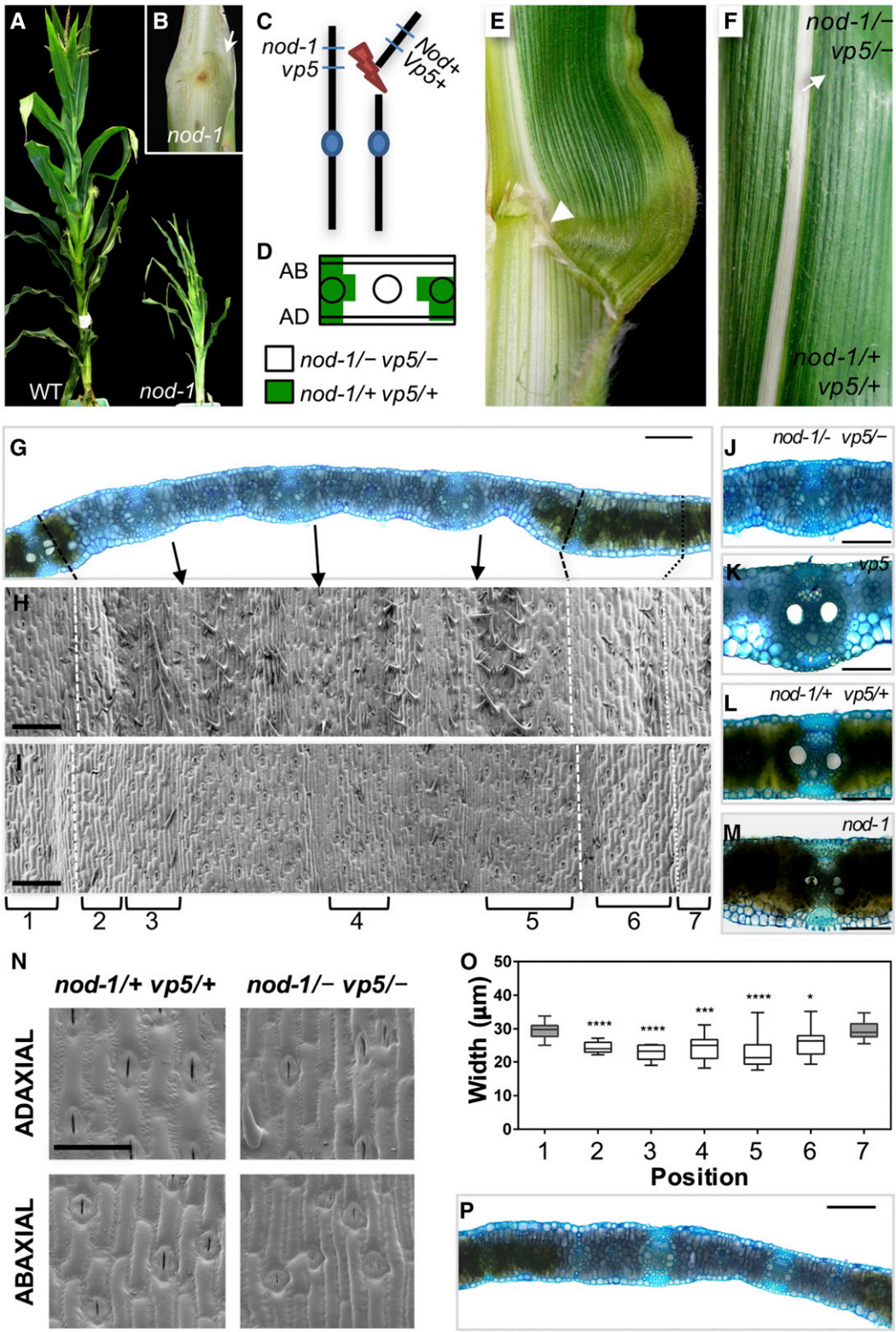

Figure 6. NOD Functions Cell Autonomously in the Leaf Blade.

(A) Wild-type and *nod-1* F2 plants following crosses of *vp5*/+ to *nod-1*/+.
(B) Sheath-blade phenotype of a *nod-1* plant in the same population. Arrow, ligule.

up- and downregulated groups, respectively (Supplemental Data Set 3). These changes could explain only ~5% (215 of 4137 genes) of *nod1* DE, indicating that the extended juvenility is not the major factor behind *nod-1* global differential expression.

Genes involved in the gibberellin (GA) pathway, which are known to regulate growth (Claeys et al., 2014), were overrepresented as downregulated in *nod-1* (Figure 7A). A defect in the GA pathway is conserved in a rice MCA mutant, *pad* (Liu et al., 2015). To test if GA deficiency is causal to the *nod-1* phenotypes, we applied exogenous GA_3 to 2-week-old plants. The treatment rescued the GA biosynthesis-deficient mutant *d1* (Chen et al., 2014) but not the GA insensitive *D9* mutant (Lawit et al., 2010). In *nod-1*, GA_3 application caused a small increase in stem height, but failed to rescue the other pleiotropic phenotypes (Supplemental Figures 7E and 7F). This finding suggests that GA deficiency is not a major factor in establishment of *nod-1* phenotypes. The reduction in expression of cell cycle genes is expected in a mutant with reduced cell proliferation. Indeed, cell cycle-regulated genes (Avramova et al., 2015) were downregulated in *nod-1*, although some only mildly (1.5-fold change). Interestingly, the expression of *tangled1*, a gene required for the proper establishment of the division plane during cell division (Walker et al., 2007), was also reduced. This could explain the abnormal cell shapes observed in *nod-1*.

The MapMan category stress response was highly enriched among *nod-1* upregulated transcripts. Included in this broad category are "touch and wounding" and "biotic stress." Indeed, multiple transcriptional changes in *nod-1* could be explained by a constitutive upregulation of the pathogen response (Figures 7A and 7B). Among those are the upregulation of genes encoding various receptor-like kinases, secondary metabolites (e.g., flavonoids), and multiple transcription factors (e.g., WRKYs) (Verma et al., 2016). Salicylic acid and jasmonic acid are only mildly overrepresented ($P < 0.05$) in upregulated and downregulated *nod-1* genes, respectively. *nod-1* also recapitulates changes in carbon metabolism-related genes known to occur during biotic stress responses (Huot et al., 2014), with a downregulation of starch biosynthesis and upregulation of invertase genes (Supplemental Figure 7G). Conversely, starch levels are reduced in mutant plants (Supplemental Figure 7H). Various gene families associated with the oxidative burst are overrepresented in *nod-1*, including peroxidases, glutaredoxin, and glutathione *S*-transferases (Figure 7B), although we did not observe hypersensitive response lesions. Staining for hydrogen peroxide and superoxide confirmed the production of reactive oxygen species (ROS) in *nod-1* leaves (Figures 7C and 7D), a known response to stress.

As cell wall-related genes are also overrepresented in *nod-1* (Figure 7B) and Arabidopsis MCA1 was shown to be involved in the cell wall stress response pathway (Wormit et al., 2012; Denness et al., 2011), we investigated the composition of wild-type and *nod-1* cell walls. The levels of hemicellulosic-based arabinose are increased in *nod-1*, while hemicellulosic xylan and cellulose levels are unchanged (Supplemental Figure 4E). Both transcription and cell wall sugar composition are consistent with a stress response (Le Gall et al., 2015; Tenhaken, 2015). The exception is the reduction in lignin content observed by phloroglucinol staining in leaf and stem tissues (Supplemental Figures 4A to 4D) and correlated with the downregulation of the phenylpropanoid category (Figure 7B). A significant but only minor reduction in both lignin content and composition (Supplemental Figure 4F) indicates that overall lignification is not altered in the *nod-1* mutant and that the changes in staining are likely due to cell differentiation defects (Figure 4).

In summary, the transcriptome analysis confirmed changes in the juvenile-to-adult transition and patterning pathways in the *nod-1* mutant. Additionally, we detected the enrichment of hormone metabolism, cell wall, and stress categories. Surprisingly, *nod* has transcriptional changes consistent with the upregulation of pathogen defenses.

DISCUSSION

We identified and characterized the maize *nod* mutant, which shows pleiotropic defects in growth and cell differentiation. NOD (previously known as CNR13) is the maize homolog of MCA1 and MCA2 (Nakagawa et al., 2007; Yamanaka et al., 2010). Like MCA homologs, NOD localized to the plasma membrane when transiently expressed in wild tobacco. MCA deficiency causes a reduction in overall organ size in Arabidopsis (Yamanaka et al., 2010), rice (Liu et al., 2015; Kurusu et al., 2012a), and maize (this

Figure 6. (continued).

(C) Genetic design for production of *nod-1* mosaics in which random chromosome breaks that are proximal to *Vp5*+ create *nod-1* mutant sectors marked by the linked *vp5* albino allele.

(D) Composition of analyzed sectors. *nod-1*/− *vp5*/− are hemizygous for both genes; *nod-1*/+ *vp5*/+ are heterozygous for both genes.

(E) Sheath-blade region of leaf containing *nod-1 vp5*/− sector. Arrow, smaller and interrupted ligule.

(F) Sector in blade region.

(G) TBO stained cross section through sector in **(F)**. Bar = 200 μm.

(H) and **(I)** Scanning electron micrograph of adaxial **(H)** and abaxial **(I)** region corresponding to **(G)**. Bar = 200 μm.

(J) to **(M)** TBO stained cross section through blades of different genotypes. Bar = 200 μm.

(N) Detail of adaxial and abaxial regions of **(H)** and **(I)**. Bar = 50 μm.

(O) Width of cells in regions 1 to 7 of **(G)** to **(I)**. Regions 1 and 7 are green, fully wild-type regions, 2 and 6 have wild-type (green) and mutant (albino) layers, 3 and 5 are the first fully albino regions at the border, and 4 is fully albino. Data represent distribution of values. $n = 3$ leaf regions (more than 10 cells each). $^*P \leq 0.05$; $^{***}P \leq 0.001$, $^{****}P \leq 0.0001$, unpaired two-sample Student's *t* tests.

(P) Example of another mutant sector. The composition is the same as in **(D)** but inverted horizontally. Bar = 200 μm.

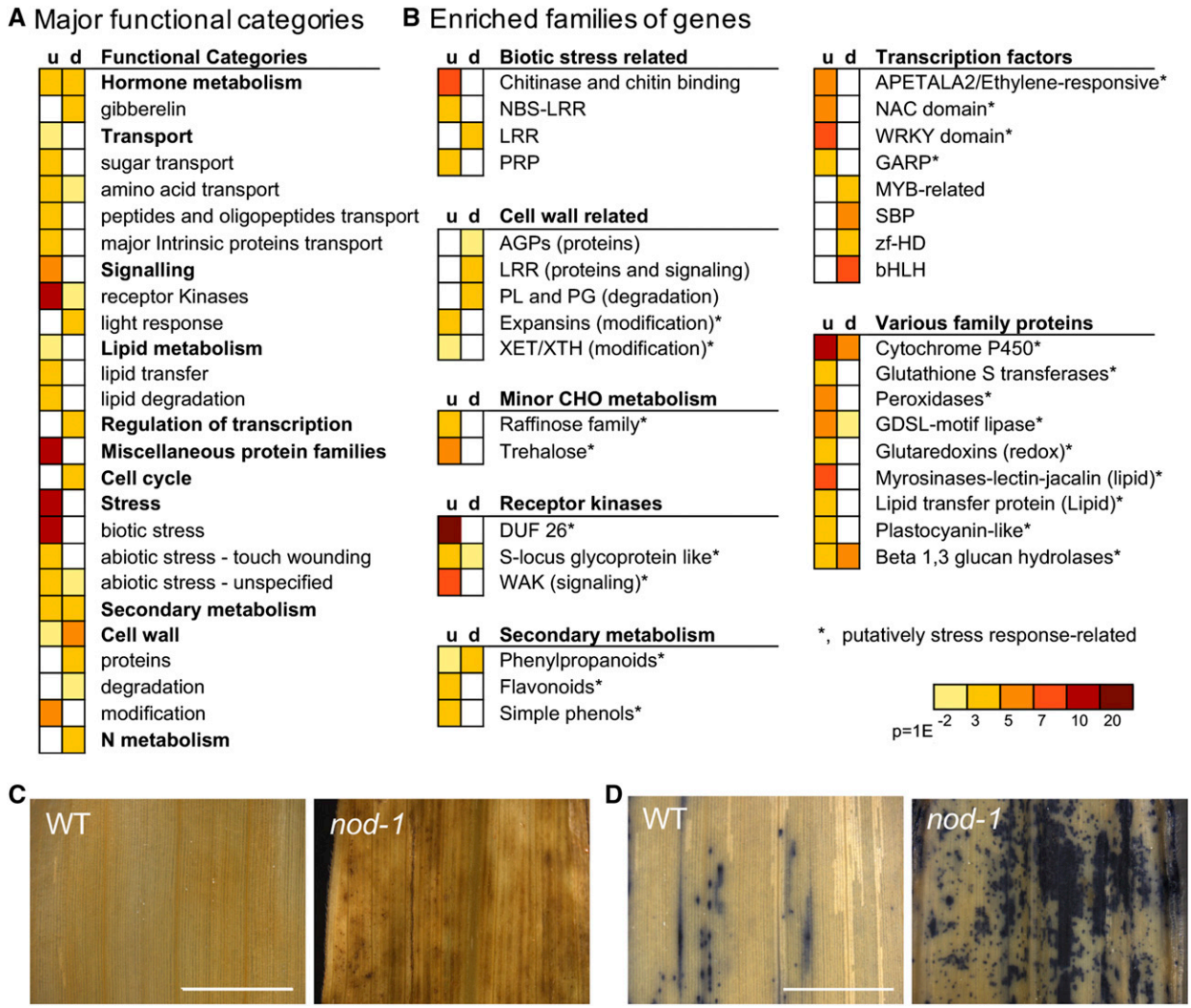

Figure 7. MapMan Functional Categories Enriched in *nod-1* DE Gene Data Set.

(A) Enrichment of functional categories. u and d, upregulated and downregulated genes, respectively.
(B) Enrichment of gene families.
(C) H_2O_2 accumulation in wild-type and *nod-1* leaves stained in brown. Bar = 0.5 cm.
(D) Superoxide accumulation in wild-type and *nod-1* leaves stained in blue. Bar = 0.5 cm.

study). Hence, MCA appears to be not only conserved in sequence, but also, at least partially, in function. Nevertheless, severe organ patterning defects have only been reported in *nod* mutants.

MCAs were shown to complement the mating-induced, low calcium uptake and lethality phenotypes of components of the Cch1/Mid1 high-affinity Ca^{2+} influx system. The mechanosensing phenotype of Arabidopsis *mca1* and positive effects on Ca^{2+} levels upon overexpression in various cell types have led to the hypothesis that MCAs form membrane-localized stretch-activated Ca^{2+} channels (Nakagawa et al., 2007; Yamanaka et al., 2010; Kurusu et al., 2012a, 2012b, 2012c; Furuichi et al., 2012). Like other studied MCAs (Nakagawa et al., 2007; Yamanaka et al., 2010; Kurusu et al., 2012c), NOD was able to partially complement the lethality phenotype of the *mid1* yeast mutant upon treatment with the mating hormone, further indicating functional conservation. However, we did not observe Ca^{2+} channel activity when expressing NOD in *X. laevis* oocytes using the patch clamp technique under the conditions tested. It is possible that MCAs form membrane Ca^{2+} pores dependent on the presence of additional proteins and/or that this activity relies on loading under different conditions for oligomerization (Nakano et al., 2011). Although current data point to a role connected with Ca^{2+} uptake, an indirect effect of MCAs by activating/regulating endogenous Ca^{2+} channel systems cannot be excluded (Figure 8). Future work should address the effects of NOD on calcium uptake in planta. Additionally, identification of NOD protein interactors

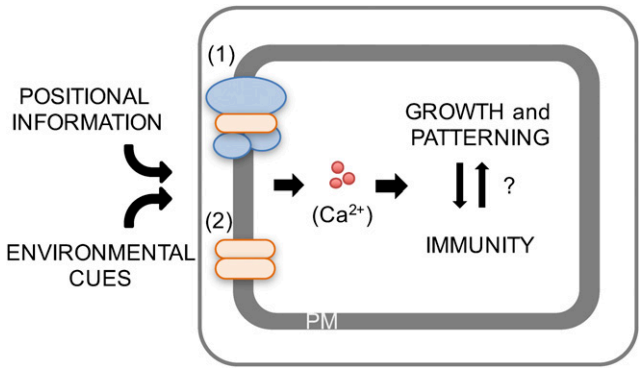

Figure 8. Model of NOD Function.

We hypothesize that NOD (yellow) localizes to the plasma membrane (PM), transducing positional and environmental information during patterning and growth of maize organs. That information might be transmitted through Ca^{2+}, with NOD either regulating Ca^{2+} channels (blue; 1) or dimerizing and forming a channel itself (2), as suggested in Arabidopsis (Nakagawa et al., 2007; Nakano et al., 2011). The information transduced by NOD regulates growth, patterning, and immunity through an unknown mechanism.

might elucidate function and possible Ca^{2+} uptake-related mechanisms.

nod mutants are impaired in cell number (proliferation), cell size (expansion), and cell differentiation. Smaller cells were also reported in the rice MCA mutant *pad* (Liu et al., 2015). Studies in tomato and maize indicated that other PLAC8-containing proteins act as cell number regulators, but with inverse correlation between size and expression levels and no effect on cell growth (Guo et al., 2010; Cong and Tanksley, 2006). MCA expression in tobacco (*Nicotiana tabacum*) cells is cell cycle regulated, and RNAi MCA rice cultured cells had low proliferation under low calcium conditions (Kurusu et al., 2012a, 2012c). While it is possible that NOD plays a role in regulating the cell cycle, it must have additional functions in cell differentiation and tissue organization, as exemplified by the stomata and ligule defects.

nod-1 mutants have several hallmarks of pathogen-induced immune responses, including accumulation of ROS, overexpression of various classes of pathogenesis-related genes, reduction in plant size, and suppression of cell division (Eichmann and Schäfer, 2015). Abnormal leaf morphologies have been observed previously in autoimmune genotypes (Du et al., 2009), and mutants in immunity-involved MAP kinases have stomata patterning defects in Arabidopsis (Khan et al., 2013), much like *nod-1*. In addition, the expressivity of *nod* in different inbreds is reminiscent of hybrid necrosis (Bomblies and Weigel, 2007; Todesco et al., 2014; Zhang et al., 2014). Ca^{2+} signals are known to regulate immune responses in plants, both positively and negatively (Verma et al., 2016; Du et al., 2009; Zhang et al., 2014), which could connect a putative NOD function in Ca^{2+} uptake or signaling to misregulation of defense pathways. However, developmental defects resulting from autoimmune responses are minimally understood in dicots and monocots, with no leaf patterning defects reported for maize autoimmune genotypes (Hu et al., 1996; Olukolu et al., 2013; Wang et al., 2015). The question remains whether *nod-1* is an autoimmune mutant with defects, for example, in *R* gene regulation, or if those transcriptional changes are a secondary effect of its complex phenotype (Figure 8).

Arabidopsis MCA1 has a proposed role in monitoring cell wall integrity (Hamann et al., 2009; Denness et al., 2011). Interestingly, cell wall synthesis inhibition triggers pathogen response pathways and inhibits cell division and expansion (Hamann, 2015). Disturbance of the cell cycle is also known to trigger pathogen responses (Bao et al., 2013). Cell wall synthesis CSDL mutants, *warty* and *slender leaf*, have overlapping phenotypes with *nod-1*, including reduced organ size, defects in cell division, and abnormal stomata differentiation (Hunter et al., 2012; Yoshikawa et al., 2013). Given that the cell wall composition of mature *nod-1* tissues was nearly unchanged, it is unlikely that NOD contributes to cell wall synthesis, while a role in cell wall signaling cannot be excluded.

A growing body of literature suggests that plant shape is determined at the supracellular level and not solely determined by individual cells. For example, leaf shape is normal in mutants with altered cell division patterns, such as *tangled* or *warty* (Smith et al., 2001; Reynolds et al., 1998). In maize, leaf shape is uniform through development but undergoes an enormous increase in size, from 10 to 150 cm in later leaves. This massive growth must be integrated with information required to produce a leaf that is asymmetric relative to three axes of growth. *nod-1* plants have reduced organ growth and abnormal cell shapes, as seen in both *tangled* and *warty*, but additionally fail to produce organs with the correct axial information. Interestingly, the function of NOD in proximal-distal leaf patterning is not restricted to establishing a border between sheath and blade or elaborating ligule and auricle, as seen in other liguleless mutants, such as *lg2* or *Lgn* (Moon et al., 2013; Harper and Freeling, 1996). Instead, at the ligule, NOD is involved in the perception of patterning signals, downstream of LG1, and translating them into specific decisions in cell fate. Our mosaic analysis is consistent with a role for NOD in decoding the patterning and differentiation information in developing tissues. The defect is mostly postmeristematic, as shown by the correct KN1 localization and function and by the observation that a tassel that initiated normally failed when patterning and growth initiated. Thus, NOD may be required to maintain tissue patterning, coordinating the actions at a cellular level with that of the organ as a whole. This function may explain why early (smaller) leaves have milder defects.

As organogenesis is influenced by both intrinsic and extrinsic cues, it is possible that NOD is also required to integrate environmental information into the developmental program (Figure 8). Abnormal signaling or perception of external cues leads to both a developmental and pathogen response. The analysis of *nod-1* in inbred backgrounds that permit more normal architecture (Supplemental Figure 2), but still have patterning and cellular defects, will elucidate the connection of NOD to pathogen responses. Understanding the connection between development, immunity, and cell wall integrity will lead to an understanding of NOD function, and, in a broader sense, of all MCA proteins.

METHODS

Mapping, Plant Materials, and Phenotypic Analysis

The maize (*Zea mays*) *nod-1* mutant was identified in an F2 family (04HI-A619xB73-GN156) following EMS mutagenesis of B73 pollen crossed onto A619 ears. Mutants were crossed to A619 and then sib-crossed to generate families that segregated 50% *nod-1*/A619 and 50% *nod-1*/*nod-1*. 50 recombinants were found using 700 individuals, limiting the region to four genes located between 11,945 and 12,125 kb on the short end of chromosome 1. *nod-1* mutants were introgressed into B73 at least four times before analysis. Wild type refers to normal siblings of the same family. All phenotypes were scored in the greenhouse. Blade length of the leaf above the top ear was measured along the midrib, from ligule to tip, and width was measured at the midpoint of the length. Stem height was measured from the soil to the insertion point of the tassel. Analysis was performed on 10 individual plants for each genotype.

Histology and Immunolocalization

For analysis of SAMs, 3-week-old shoots were dissected and fixed in FAA with vacuum infiltration, dehydrated in an ethanol series, treated with Histo-Clear, and embedded in Paraplast plus. After sectioning as described before (Jackson, 1991), the slides where dewaxed in Histo-Clear and rehydrated. The slides were stained in 0.05% TBO or used for immunolocalization. Immunolocalization was performed as previously described (Jackson, 1991), using KN1 (Bolduc and Hake, 2009) and LG1 (Lewis et al., 2014) antibodies, both at 1:500 dilution. Slides were photographed with a Leica bright-field microscope (DM 4000 B). For measurement of SAM, 10 longitudinal TBO-stained sections of individual shoots were used and the size determined in ImageJ with the "measure" tool.

Whole-mount leaf preparations (each with ~1 cm^2 of area) were cleared according to Chuck et al. (1996), stained with 0.05% TBO, and observed with bright-field microscopy. Hand sections of leaves were mounted in water and observed under UV using a 365-nm excitation filter and a 420-nm long pass emission filter or stained with 0.05% TBO and observed with light microscopy. Fluorescent pictures were analyzed in image J where the blue and green channels were pseudocolored to gray. The size of interstomatal epidermal cells of leaf 4 was determined using the ImageJ (Schneider et al., 2012) "measure" tool. To determine width and length, we used pictures of whole mount cleared leaf pieces stained in TBO. Two hundred cells of two leaves from different plants were measured per genotype. The thickness was determined in pictures of hand sections and 40 cells from three leaves of different plants were measured. Quantification of stomata abnormalities was conducted in Image J with the "Cell Counter" tool, using pictures of whole-mount preparations of leaf 12. Two hundred stomata from each of three to six leaves from different plants per data point were analyzed. Stomata density was measured in six regions of individual leaves.

Scanning electron microscopy was performed as described before (Thompson et al., 2014). Blades of adult, mature leaves were stained to detect hydrogen peroxide or superoxide ROS (Kumar et al., 2014). Three to five blades were analyzed per genotype. Replicas of the surface of developing leaves were obtained as described before (Moon et al., 2013) and then mounted for scanning electron microscopy.

Fresh-cut sections of leaf blade or stem were stained with Wiesner's solution (2% [w/v] phloroglucinol in ethanol:50% HCl [v/v] in water [95:5, v/v]) and immediately observed and photographed using a bright-field microscope.

Antibody Creation and Protein Gel Blot Analysis

The NOD antibody was created as described before (Chuck et al., 2010). The cDNA sequence excluding the first putative transmembrane was amplified with primers NOD01-F and NOD01-R and cloned into pENTR and then into pDEST15 or pDEST17 according to manufacturer's instructions (Invitrogen). All primer sequences are listed in Supplemental Table 1. NOD proteins were produced in *Escherichia coli*, purified using a N-terminal His-tag, and used for immunization of guinea pigs (Cocalico Biologicals). The serum was affinity purified against an N-terminal GTS-tagged NOD fusion protein.

Transcript and Protein Analysis

Total RNA was isolated from shoot apices with leaf primordia tissues using the PureLink Micro-to-Midi Total RNA Purification System (Ambion) according to the manufacturer's instructions. cDNA was synthesized using 1 μg of RNA, oligo dT(20), and SSIII RT reverse transcriptase (Invitrogen) according to the manufacturer's instructions, on three independent replicates, each corresponding to five apices. qPCR was performed for each cDNA replicate, and all samples were run in duplicate. PCRs were performed using GoTaq DNA Polymerase (Promega) and labeled with EvaGreen dye (Biotium), under the following conditions: 95°C for 10 min, 40 cycles of 95°C for 15 s, 60°C for 1 min, and a final melt curve stage from 60 to 95°C. Primers used to amplify NOD are P01-F and P01-R. Data were normalized using *ZmGAPDH* as the reference gene. The CFX96 real-time PCR detection system (Bio-Rad) was used. Gene expression was normalized by subtracting the CT value of the control gene from the CT value of the gene of interest. Average expression ratios were obtained from the equation $2^{-\Delta\Delta CT}$, where ΔΔCT represents ΔCT (gene of interest in stage evaluated) – ΔCT (gene of interest at control stage), according to the protocol reported by Czechowski et al. (2004).

The TMHMM (CBS of DTU, Technical University of Denmark; www.cbs.dtu.dk/services/TMHMM), SMART (University of Heidelberg; smart.embl-heidelberg.de), and InterProScan (EMBL-EBI; www.ebi.ac.uk/Tools/pfa/iprscan) bioinformatics tools were used to analyze protein sequences and identify conserved motifs.

Phylogenetic Analysis

Alignments were done with protein-coding sequences by the neighbor-joining method using ClustalW (2.1). The alignment in Supplemental Figure 6 was built with Boxshade. The phylogenetic tree was produced with Mega7 using bootstrap analysis with 1000 replications. The tree is drawn to scale, with branch lengths in the same units as the evolutionary distances used. The aligned sequences used to construct the phylogenetic tree are shown in Supplemental File 1.

NOD Immunodetection

Standard SDS-PAGE (12% acrylamide gel) was performed with protein extracts of 100 mg of ground tissue from maize shoot apices using 200 μL of 1× SDS loading buffer. Semidry transfer, blocking, and incubation with 1:2000 affinity-purified guinea pig polyclonal antibody anti-NOD was performed. NOD protein was detected using chemiluminescence with 1:3000 anti-GP secondary HRP-coupled antibody (Santa Cruz Biotechnology). After NOD detection, membranes were stripped and tubulin was detected as a loading control by incubation with 1:25,000 monoclonal anti-TUB. Detection was done using 1:10,000 secondary HRP-coupled antibody (Santa Cruz Biotechnology).

Transient Expression in Wild Tobacco

The full-length NOD coding sequence was amplified from cDNA with primers NOD02-F and NOD01-R, cloned into pENTR and then into pEarley101 (Earley et al., 2006) using the Gateway method, according to the manufacturer's instructions (Invitrogen). The construct was transformed into *Agrobacterium tumefaciens* strain GV3101. Transient transformation of wild tobacco (*Nicotiana benthamiana*) was performed as described (Bolduc and Hake, 2009). This experiment was repeated three times.

Yeast Lethality Assay

All strains were derived from haploid W303a. *mid1* mutants were generated by replacing the MID1 open reading frame with the Kan resistance gene

from pKanMX4 and transformed using standard yeast transformation techniques. Primers used were MID1-KanMX-fw and MID1-KanMX-rv. MID1, NOD, and NOD-2 expression strains were derived from a set of yeast single integration vectors containing selectable markers and targeting sequences for the LEU2 locus. Expression vectors were amplified by PCR and transformed using standard yeast transformation techniques. MID1 sequence was amplified from *Saccharomyces cerevisiae* genomic DNA, using primers scMID1-fwd and scMID1-rev, and inserted into *Xho*I/*Bam*HI-digested pMC02. NOD and NOD-2 were amplified from maize cDNA using primers zmNOD-fwd and zmNOD-rev. Amplification primers used were LEU-fw and Leu-rv. The cells were grown in YPD at 30°C.

Prior to the experiment, the cells were grown and maintained in exponential phase for ~24 h in SD-Ca100 (Iida et al., 1994) and then diluted to an optical density (OD_{600}) of 0.02. After 2 h, the cells were centrifuged and resuspended in SD-Ca (Iida et al., 1994) with and without α-Factor mating pheromone (Zymo Research; 20 μM). After 3 h of treatment at 30°C, the cells were centrifuged and resuspended in 1× TE and LIVE/DEAD FungaLight. The Yeast Viability protocol was performed as suggested by the manufacturer (Molecular Probes).

For the flow cytometry analysis, fluorescence measurements were performed on an LSRII analyzer (BD Biosciences). A blue (488 nm) laser was used to excite S9, and a green (561 nm) laser was used to excite PI. Emission was detected using a 530/30-nm band-pass filter for S9 (Chroma) and a 610/20 band-pass filter for PI (Chroma). Ten thousand cells were collected for each measurement. Flow cytometry data were analyzed in MATLAB (Mathworks).

Oocyte Experiments

The *nod*, *nod-2* (mutant), *AtCIPK23*, *AtCBL1*, and *AtAKT1* cDNA was subcloned into pGEMHE. The capped RNA (cRNA) was synthesized from 1 μg of linearized plasmid DNA template using an mMessage mMachine in vitro transcription kit (Ambion) according to the manufacturer's recommendations. The cRNA quality was checked by agarose gel electrophoresis. The concentration was determined by A_{260}/A_{280} and adjusted to a final concentration of 0.5 μg/μL. A total 11.5 ng of each tested cRNA was injected into each oocyte. Injected oocytes were incubated in ND96 at 18°C for 2 d prior to electrophysiological analysis. Oocytes were voltage clamped using a TEV 200 amplifier (Dagan) and monitored by computer through a Digidata 1550 A/D converter and pCLAMP 10.2 software (Axon Instruments). The pipette solution contained 3 M KCl. The isotonic perfusion buffer contains 40 mM KCl, 2 mM EGTA, and 5 mM HEPES, pH 7.5 adjusted with KOH, 220 mOsmol/L adjusted with D-mannitol. The hypoosmotic solution contains 40 mM KCl, 2 mM EGTA, and 5 mM HEPES, pH 7.5 adjusted with KOH, 110 mOsmol/L adjusted with D-mannitol. The membrane voltage was stepped to potentials starting at +40 to −140mV for 0.8 s with 20-mV decrements and the holding potential was 0 mV. This experiments was performed six times.

Genetic Mosaic Analysis

The *vp5* cell-autonomous mutant (Robichaud et al., 1979; Becraft et al., 2002) was used as a recessive marker in the mosaic analysis. The *vp5* segregating population, in a Hi27 background, was provided by the Maize Coop Stock Center (Urbana, IL; stock 103D). *vp5* is located on the top arm of chromosome 1, 5.6 Mb proximal to *nod*. We crossed *vp5*/+ to *nod*-1/+, recovered two F1 individuals segregating both mutations and propagated them to F3. We scored a total of 23 F3 families for linked mutant alleles. Four families were positively identified and used in the analysis. Irradiation treatments were performed on seeds imbibed for 3 d on wet filter paper at 25°C. An x-ray tube (CXR-105 x-ray tube; Comet Technologies) was powered at 62 kV, 9 mA, with the x-ray window positioned 108 mm from the center of the sample plate. The applied dose was determined with a radiation measurement system (Accu-Dose MNL/2086; Radcal) using a high-dose-rate ion chamber (10X6-0.18; Radcal). An exposure time of 2 min produced a mean target dose of 10 Gy, with a maximum of 15 Gy at the center and minimum of 5.8 Gy at the edge of the plate. After irradiation, the germinated seedlings were transplanted and field grown at Gill Tract (Albany, CA) until maturity and then analyzed.

RNA Sequencing Analysis

Ten shoots of each genotype were dissected (Supplemental Figures 7A and 7B) and used for RNA extraction. Triplicate pools of 10 shoot apices each were harvested from normal siblings and *nod-1* mutants. Total RNA was extracted using Trizol (Life Technologies) according to the manufacturer's instructions. mRNA was purified from 3 μg of total RNA using Dynabeads oligo(dT) (Thermo Fisher Scientific) by two successive purifications. mRNA was used for library construction using the ScriptSeq v2 RNaseq system (Epicentre). Addition of bar-coded adapters enabled multiplexed sequencing. The size distribution of the libraries was verified on a high sensitivity Bioanalyzer chip.

Sequenced reads were aligned to the maize genome (B73 Refgen V3) using TopHat2 (Kim et al., 2013). HTseq (Anders and Huber, 2010) was used to obtain the raw read values for each gene. Genes with count number lower than 10 were excluded from the analysis. The Bioconductor edgeR package was used to identify differentially expressed genes (Robinson et al., 2010), using the Benjamin and Hochberg method for determining the FDR. Functional analysis of DE genes was done using MapMan gene annotation (Thimm et al., 2004), and enrichment of categories was determined with the binomial test using a P value < 0.01, only in categories with more than five DE genes.

Exogenous Application of GA_3

Wild-type, *nod-1*, *d1*, and *D9* greenhouse-grown seedlings were treated with a 100 μM GA_3 aqueous solution containing 0.1% Tween 20. Mock solution with no GA_3 was used as a control. The treatment was started 12 d after sowing by adding 100 μL of each solution to the inner whorls of seedlings. Applications were done three times a week with measurements every other day. Ten wild-type or *nod-1* seedlings were used for each experimental data point. Three *d1* and *D9* were used as controls. Stem length was measured from the base of the stem to the last emerged ligule.

Cell Wall Composition and Starch Analysis

Two-week-old plant tissue was freeze-dried and homogenized to a fine powder using a mixer mill (MM400; Retsch Technology) at 30 Hz for 2 min. One milligram of destarched cell wall extracts per assay was used for the determination of cellulose content, total lignin content, and monolignol composition (Foster et al., 2010a, 2010b). For the determination of matrix polysaccharide composition, 1 mg of destarched AIR was hydrolyzed in 2 M TFA for 90 min at 121°C. A Shimadzu Prominence HPLC system equipped with a refractive index detector was used to measure glucose, xylose, and arabinose in the hydrolysate. Samples were separated with a Phenomenex RezexTM RFQ-Fast Acid H+ (8%) ion exchange column (100 × 7.8 mm) and a Bio-Rad Cation H guard column (30 × 4.6 mm) with 5 mM sulfuric acid as the mobile phase and a flow rate of 1.0 mL min^{-1} at 55°C for 5 min.

Statistical Analysis

Unpaired Student's *t* tests were used to determine significance between populations. Graphs throughout the article show the mean value and error bars the SD.

Accession Numbers

Sequence data from this article can be found in the Arabidopsis Genome Initiative or GenBank/EMBL databases; all accession numbers for genes mentioned in this study are given in Supplemental Data Set 2.

Supplemental Data

Supplemental Figure 1. *nod-1* cells are smaller than the wild type.

Supplemental Figure 2. Severity of *nod* mutant phenotypes varies with genetic background.

Supplemental Figure 3. *nod-1* has proximal-distal patterning defects.
Supplemental Figure 4. Cell wall analysis of *nod-1* leaves.
Supplemental Figure 5. *nod-1* has defects in stomata development.

Supplemental Figure 6. Phylogenetic analysis of *nod*.

Supplemental Figure 7. Comparison of differential gene expression between *nod-1* and the wild type.

Supplemental Table 1. List of primers used in this study.

Supplemental Data Set 1. Alignment statistics.

Supplemental Data Set 2. List of genes in the RNA-seq data set.

Supplemental Data Set 3. Overlap of *nod-1* DE genes and primordial leaf (Johnston et al., 2014), KN1 (Bolduc et al., 2012b), and juvenile/adult (Beydler et al., 2016) data sets.

Supplemental File 1. Alignment data used for phylogenetic analysis.

ACKNOWLEDGMENTS

We thank Devi Santhosh and Jessica Rodriquez for mapping, Gillian Xu for technical assistance, Jake Brunkard for discussions about autoimmunity, all Hake lab members for comments and criticisms, De Wood and Tina Williams for the USDA-ARS microscope facility, Lia Poasi and her greenhouse staff for expert care of the plants, and Eric Jackson at the USDA-ARS facility for seed irradiation. The work was supported by NSF IOS-1238202 to S.H., UC-MEXUS CONACYT to M.J.A.-J., Marie Curie PIOF-GA-2013-623553 to V.R., and the Office of Science (BER), U.S. Department of Energy, Grant DE-SC001240 to M.P.

AUTHOR CONTRIBUTIONS

M.R. and S.H. designed this work. M.J.A.-J. performed qRT-PCR, protein gel blot analysis, hormone treatments, and RNA-seq library preparation. M.W.L. made the NOD antibody. J.P.F. performed yeast experiments. W.T. performed oocyte experiments. V.R. performed the cell wall and starch analysis. M.R. carried out all other experiments. M.R., M.J.A.-J., S.L., M.P., and S.H. analyzed the data. M.R. and S.H. wrote the manuscript.

Received November 28, 2016; revised February 13, 2017; accepted February 27, 2017; published March 2, 2017.

REFERENCES

Anders, S., and Huber, W. (2010). Differential expression analysis for sequence count data. Genome Biol. **11:** R106.

Avramova, V. AbdElgawad, H., Zhang, Z., Fotschki, B., Casadevall, R., Vergauwen, L., Knapen, D., Taleisnik, E., Guisez, Y., Asard, H., and Beemster, G.T.S. (2015). Drought induces distinct growth response, protection and recovery mechanisms in the maize leaf growth zone. Plant Physiol. **169:** 1382–1396.

Bao, Z., Yang, H., and Hua, J. (2013). Perturbation of cell cycle regulation triggers plant immune response via activation of disease resistance genes. Proc. Natl. Acad. Sci. USA **110:** 2407–2412.

Becraft, P.W., Bongard-Pierce, D.K., Sylvester, A.W., Poethig, R.S., and Freeling, M. (1990). The *liguleless-1* gene acts tissue specifically in maize leaf development. Dev. Biol. **141:** 220–232.

Becraft, P.W., Li, K., Dey, N., and Asuncion-Crabb, Y. (2002). The maize *dek1* gene functions in embryonic pattern formation and cell fate specification. Development **129:** 5217–5225.

Beydler, B.D., Osadchuk, K., Cheng, C.-L., Manak, J.R., and Irish, E.E. (2016). The juvenile phase of maize sees upregulation of stress-response genes and is extended by exogenous JA. Plant Physiol. **171:** 2648–2658.

Bolduc, N., and Hake, S. (2009). The maize transcription factor KNOTTED1 directly regulates the gibberellin catabolism gene *ga2ox1.* Plant Cell **21:** 1647–1658.

Bolduc, N., O'Connor, D., Moon, J., Lewis, M., and Hake, S. (2012a). How to pattern a leaf. Cold Spring Harb. Symp. Quant. Biol. **77:** 47–51.

Bolduc, N., Yilmaz, A., Mejia-Guerra, M.K., Morohashi, K., O'Connor, D., Grotewold, E., and Hake, S. (2012b). Unraveling the KNOTTED1 regulatory network in maize meristems. Genes Dev. **26:** 1685–1690.

Bomblies, K., and Weigel, D. (2007). Hybrid necrosis: autoimmunity as a potential gene-flow barrier in plant species. Nat. Rev. Genet. **8:** 382–393.

Candela, H., and Hake, S. (2008). The art and design of genetic screens: maize. Nat. Rev. Genet. **9:** 192–203.

Chen, Y., Hou, M., Liu, L., Wu, S., Shen, Y., Ishiyama, K., Kobayashi, M., McCarty, D.R., and Tan, B.-C. (2014). The maize *DWARF1* encodes a gibberellin 3-oxidase and is dual localized to the nucleus and cytosol. Plant Physiol. **166:** 2028–2039.

Chuck, G., Lincoln, C., and Hake, S. (1996). *KNAT1* induces lobed leaves with ectopic meristems when overexpressed in Arabidopsis. Plant Cell **8:** 1277–1289.

Chuck, G., Cigan, A.M., Saeteurn, K., and Hake, S. (2007). The heterochronic maize mutant *Corngrass1* results from overexpression of a tandem microRNA. Nat. Genet. **39:** 544–549.

Chuck, G., Whipple, C., Jackson, D., and Hake, S. (2010). The maize SBP-box transcription factor encoded by *tasselsheath4* regulates bract development and the establishment of meristem boundaries. Development **137:** 1243–1250.

Claeys, H., De Bodt, S., and Inzé, D. (2014). Gibberellins and DELLAs: central nodes in growth regulatory networks. Trends Plant Sci. **19:** 231–239.

Cong, B., and Tanksley, S.D. (2006). FW2.2 and cell cycle control in developing tomato fruit: a possible example of gene co-option in the evolution of a novel organ. Plant Mol. Biol. **62:** 867–880.

Czechowski, T., Bari, R.P., Stitt, M., Scheible, W.-R., and Udvardi, M.K. (2004). Real-time RT-PCR profiling of over 1400 Arabidopsis transcription factors: unprecedented sensitivity reveals novel root- and shoot-specific genes. Plant J. **38:** 366–379.

Denness, L., McKenna, J.F., Segonzac, C., Wormit, A., Madhou, P., Bennett, M., Mansfield, J., Zipfel, C., and Hamann, T. (2011). Cell wall damage-induced lignin biosynthesis is regulated by a reactive oxygen species- and jasmonic acid-dependent process in Arabidopsis. Plant Physiol. **156:** 1364–1374.

Du, L., Ali, G.S., Simons, K.A., Hou, J., Yang, T., Reddy, A.S.N., and Poovaiah, B.W. (2009). Ca^{2+}/calmodulin regulates salicylic-acid-mediated plant immunity. Nature **457:** 1154–1158.

Dudley, M., and Poethig, R.S. (1993). The heterochronic *Teopod1* and *Teopod2* mutations of maize are expressed non-cell-autonomously. Genetics **133:** 389–399.

Earley, K.W., Haag, J.R., Pontes, O., Opper, K., Juehne, T., Song, K., and Pikaard, C.S. (2006). Gateway-compatible vectors for plant functional genomics and proteomics. Plant J. **45:** 616–629.

Eichmann, R., and Schäfer, P. (2015). Growth versus immunity–a redirection of the cell cycle? Curr. Opin. Plant Biol. **26:** 106–112.

Facette, M.R., and Smith, L.G. (2012). Division polarity in developing stomata. Curr. Opin. Plant Biol. **15:** 585–592.

Fischer, M., Schnell, N., Chattaway, J., Davies, P., Dixon, G., and Sanders, D. (1997). The *Saccharomyces cerevisiae* CCH1 gene is involved in calcium influx and mating. FEBS Lett. **419:** 259–262.

Foster, C.E., Martin, T.M., and Pauly, M. (2010a). Comprehensive compositional analysis of plant cell walls (lignocellulosic biomass) part I: lignin. J. Vis. Exp. **pii:** 1745.

Foster, C.E., Martin, T.M., and Pauly, M. (2010b). Comprehensive compositional analysis of plant cell walls (lignocellulosic biomass) part II: carbohydrates. J. Vis. Exp. **pii:** 1837.

Foster, T., Hay, A., Johnston, R., and Hake, S. (2004). The establishment of axial patterning in the maize leaf. Development **131:** 3921–3929.

Frary, A., Nesbitt, T.C., Grandillo, S., Knaap, E., Cong, B., Liu, J., Meller, J., Elber, R., Alpert, K.B., and Tanksley, S.D. (2000). *fw2.2*: a quantitative trait locus key to the evolution of tomato fruit size. Science **289:** 85–88.

Furuichi, T., Iida, H., Sokabe, M., and Tatsumi, H. (2012). Expression of Arabidopsis MCA1 enhanced mechanosensitive channel activity in the *Xenopus laevis* oocyte plasma membrane. Plant Signal. Behav. **7:** 1022–1026.

Guo, M., Rupe, M.A., Dieter, J.A., Zou, J., Spielbauer, D., Duncan, K.E., Howard, R.J., Hou, Z., and Simmons, C.R. (2010). *Cell Number Regulator1* affects plant and organ size in maize: implications for crop yield enhancement and heterosis. Plant Cell **22:** 1057–1073.

Hamann, T. (2015). The plant cell wall integrity maintenance mechanism–a case study of a cell wall plasma membrane signaling network. Phytochemistry **112:** 100–109.

Hamann, T., Bennett, M., Mansfield, J., and Somerville, C. (2009). Identification of cell-wall stress as a hexose-dependent and osmosensitive regulator of plant responses. Plant J. **57:** 1015–1026.

Harper, L., and Freeling, M. (1996). Interactions of *liguleless1* and *liguleless2* function during ligule induction in maize. Genetics **144:** 1871–1882.

Hu, G., Richter, T.E., Hulbert, S.H., and Pryor, T. (1996). Disease lesion mimicry caused by mutations in the rust resistance gene *rp1.* Plant Cell **8:** 1367–1376.

Hunter, C.T., Kirienko, D.H., Sylvester, A.W., Peter, G.F., McCarty, D.R., and Koch, K.E. (2012). *Cellulose Synthase-Like D1* is integral to normal cell division, expansion, and leaf development in maize. Plant Physiol. **158:** 708–724.

Huot, B., Yao, J., Montgomery, B.L., and He, S.Y. (2014). Growth-defense tradeoffs in plants: a balancing act to optimize fitness. Mol. Plant **7:** 1267–1287.

Iida, H., Furuichi, T., Nakano, M., Toyota, M., Sokabe, M., and Tatsumi, H. (2013). New candidates for mechano-sensitive channels potentially involved in gravity sensing in *Arabidopsis thaliana*. Plant Biol. (Stuttg.) **16** (suppl. 1): 39–42.

Iida, H., Nakamura, H., Ono, T., Okumura, M.S., and Anraku, Y. (1994). MID1, a novel *Saccharomyces cerevisiae* gene encoding a plasma membrane protein, is required for Ca^{2+} influx and mating. Mol. Cell. Biol. **14:** 8259–8271.

Jackson, D.P. (1991). *In situ* hybridization in plants. In Molecular Plant Pathology: A Practical Approach, D.J. Bowles, S.J. Gurr, and M. McPherson, eds (Oxford, UK: Oxford University), pp. 163–174.

Johnston, R., Wang, M., Sun, Q., Sylvester, A.W., Hake, S., and Scanlon, M.J. (2014). Transcriptomic analyses indicate that maize ligule development recapitulates gene expression patterns that occur during lateral organ initiation. Plant Cell **26:** 4718–4732.

Khan, M., Rozhon, W., Bigeard, J., Pflieger, D., Husar, S., Pitzschke, A., Teige, M., Jonak, C., Hirt, H., and Poppenberger, B. (2013). Brassinosteroid-regulated GSK3/Shaggy-like kinases phosphorylate mitogen-activated protein (MAP) kinase kinases, which control stomata development in *Arabidopsis thaliana.* J. Biol. Chem. **288:** 7519–7527.

Kim, D., Pertea, G., Trapnell, C., Pimentel, H., Kelley, R., and Salzberg, S.L. (2013). TopHat2: accurate alignment of transcriptomes in the presence of insertions, deletions and gene fusions. Genome Biol. **14:** R36.

Kumar, D., Yusuf, M., Singh, P., Sardar, M., and Sarin, N. (2014). Histochemical detection of superoxide and H_2O_2 accumulation in *Brassica juncea* seedlings. Bio Protoc. **4:** e1108.

Kurusu, T., et al. (2012a). Plasma membrane protein OsMCA1 is involved in regulation of hypo-osmotic shock-induced Ca^{2+} influx and modulates generation of reactive oxygen species in cultured rice cells. BMC Plant Biol. **12:** 11.

Kurusu, T., Iida, H., and Kuchitsu, K. (2012b). Roles of a putative mechanosensitive plasma membrane Ca^{2+}-permeable channel OsMCA1 in generation of reactive oxygen species and hypo-osmotic signaling in rice. Plant Signal. Behav. **7:** 796–798.

Kurusu, T., Kuchitsu, K., Nakano, M., Nakayama, Y., and Iida, H. (2013). Plant mechanosensing and Ca^{2+} transport. Trends Plant Sci. **18:** 227–233.

Kurusu, T., Yamanaka, T., Nakano, M., Takiguchi, A., Ogasawara, Y., Hayashi, T., Iida, K., Hanamata, S., Shinozaki, K., Iida, H., and Kuchitsu, K. (2012c). Involvement of the putative Ca^{2+}-permeable mechanosensitive channels, NtMCA1 and NtMCA2, in Ca^{2+} uptake, Ca^{2+}-dependent cell proliferation and mechanical stress-induced gene expression in tobacco (*Nicotiana tabacum*) BY-2 cells. J. Plant Res. **125:** 555–568.

Lawit, S.J., Wych, H.M., Xu, D., Kundu, S., and Tomes, D.T. (2010). Maize DELLA proteins dwarf plant8 and dwarf plant9 as modulators of plant development. Plant Cell Physiol. **51:** 1854–1868.

Le Gall, H., Philippe, F., Domon, J.-M., Gillet, F., Pelloux, J., and Rayon, C. (2015). Cell wall metabolism in response to abiotic stress. Plants **4:** 112–166.

Lewis, M.W., and Hake, S. (2016). Keep on growing: building and patterning leaves in the grasses. Curr. Opin. Plant Biol. **29:** 80–86.

Lewis, M.W., Bolduc, N., Hake, K., Htike, Y., Hay, A., Candela, H., and Hake, S. (2014). Gene regulatory interactions at lateral organ boundaries in maize. Development **141:** 4590–4597.

Libault, M., and Stacey, G. (2010). Evolution of FW2.2-like (FWL) and PLAC8 genes in eukaryotes. Plant Signal. Behav. **5:** 1226–1228.

Liu, Z., Cheng, Q., Sun, Y., Dai, H., Song, G., Guo, Z., Qu, X., Jiang, D., Liu, C., Wang, W., and Yang, D. (2015). A SNP in OsMCA1 responding for a plant architecture defect by deactivation of bioactive GA in rice. Plant Mol. Biol. **87:** 17–30.

Moon, J., Candela, H., and Hake, S. (2013). The *Liguleless narrow* mutation affects proximal-distal signaling and leaf growth. Development **140:** 405–412.

Moreno, M.A., Harper, L.C., Krueger, R.W., Dellaporta, S.L., and Freeling, M. (1997). *liguleless1* encodes a nuclear-localized protein required for induction of ligules and auricles during maize leaf organogenesis. Genes Dev. **11:** 616–628.

Muller, E.M., Locke, E.G., and Cunningham, K.W. (2001). Differential regulation of two $Ca^{(2+)}$ influx systems by pheromone signaling in *Saccharomyces cerevisiae.* Genetics **159:** 1527–1538.

Nakagawa, Y., et al. (2007). Arabidopsis plasma membrane protein crucial for Ca^{2+} influx and touch sensing in roots. Proc. Natl. Acad. Sci. USA **104:** 3639–3644.

Nakano, M., Iida, K., Nyunoya, H., and Iida, H. (2011). Determination of structural regions important for Ca^{2+} uptake activity in Arabidopsis MCA1 and MCA2 expressed in yeast. Plant Cell Physiol. **52:** 1915–1930.

Olukolu, B.A., et al. (2013). A connected set of genes associated with programmed cell death implicated in controlling the hypersensitive response in maize. Genetics **193:** 609–620.

Reynolds, J.O., Eisses, J.F., and Sylvester, A.W. (1998). Balancing division and expansion during maize leaf morphogenesis: analysis of the mutant, *warty-1.* Development **125:** 259–268.

Rigamonti, M., Groppi, S., Belotti, F., Ambrosini, R., Filippi, G., Martegani, E., and Tisi, R. (2015). Hypotonic stress-induced calcium signaling in *Saccharomyces cerevisiae* involves TRP-like transporters on the endoplasmic reticulum membrane. Cell Calcium **57:** 57–68.

Robichaud, C.S., Wong, J., and Sussex, I.M. (1979). Control of *in vitro* growth of viviparous embryo mutants of maize by abscisic acid. Genesis **1:** 325–330.

Robinson, M.D., McCarthy, D.J., and Smyth, G.K. (2010). edgeR: a Bioconductor package for differential expression analysis of digital gene expression data. Bioinformatics **26:** 139–140.

Sablowski, R., and Carnier Dornelas, M. (2014). Interplay between cell growth and cell cycle in plants. J. Exp. Bot. **65:** 2703–2714.

Schneider, C.A., Rasband, W.S., and Eliceiri, K.W. (2012). NIH Image to ImageJ: 25 years of image analysis. Nat. Methods **9:** 671–675.

Smith, L.G., Gerttula, S.M., Han, S., and Levy, J. (2001). Tangled1: a microtubule binding protein required for the spatial control of cytokinesis in maize. J. Cell Biol. **152:** 231–236.

Song, W.-Y., Choi, K.S., Kim, D.-Y., Geisler, M., Park, J., Vincenzetti, V., Schellenberg, M., Kim, S.H., Lim, Y.P., Noh, E.W., Lee, Y., and Martinoia, E. (2010). Arabidopsis PCR2 is a zinc exporter involved in both zinc extrusion and long-distance zinc transport. Plant Cell **22:** 2237–2252.

Song, W.-Y., Martinoia, E., Lee, J., Kim, D., Kim, D.-Y., Vogt, E., Shim, D., Choi, K.S., Hwang, I., and Lee, Y. (2004). A novel family of cys-rich membrane proteins mediates cadmium resistance in Arabidopsis. Plant Physiol. **135:** 1027–1039.

Stelpflug, S.C., Sekhon, R.S., Vaillancourt, B., Hirsch, C.N., Buell, C.R., de Leon, N., and Kaeppler, S.M. (2016). An expanded maize gene expression atlas based on RNA sequencing and its use to explore root development. Plant Genome **9:** 10.3835/plantgenome2015.04.0025.

Sun, S., Chen, D., Li, X., Qiao, S., Shi, C., Li, C., Shen, H., and Wang, X. (2015). Brassinosteroid signaling regulates leaf erectness in *Oryza sativa* via the control of a specific U-type cyclin and cell proliferation. Dev. Cell **34:** 220–228.

Sylvester, A.W., Cande, W.Z., and Freeling, M. (1990). Division and differentiation during normal and *liguleless-1* maize leaf development. Development **110:** 985–1000.

Tenhaken, R. (2015). Cell wall remodeling under abiotic stress. Front. Plant Sci. **5:** 771.

Thimm, O., Bläsing, O., Gibon, Y., Nagel, A., Meyer, S., Krüger, P., Selbig, J., Müller, L.A., Rhee, S.Y., and Stitt, M. (2004). MAPMAN: a user-driven tool to display genomics data sets onto diagrams of metabolic pathways and other biological processes. Plant J. **37:** 914–939.

Thompson, B.E., Basham, C., Hammond, R., Ding, Q., Kakrana, A., Lee, T.-F., Simon, S.A., Meeley, R., Meyers, B.C., and Hake, S. (2014). The *dicer-like1* homolog *fuzzy tassel* is required for the regulation of meristem determinacy in the inflorescence and vegetative growth in maize. Plant Cell **26:** 4702–4717.

Todesco, M., Kim, S.-T., Chae, E., Bomblies, K., Zaidem, M., Smith, L.M., Weigel, D., and Laitinen, R.A.E. (2014). Activation of the *Arabidopsis thaliana* immune system by combinations of common ACD6 alleles. PLoS Genet. **10:** e1004459.

Verma, V., Ravindran, P., and Kumar, P.P. (2016). Plant hormone-mediated regulation of stress responses. BMC Plant Biol. **16:** 86.

Walker, K.L., Müller, S., Moss, D., Ehrhardt, D.W., and Smith, L.G. (2007). *Arabidopsis* TANGLED identifies the division plane throughout mitosis and cytokinesis. Curr. Biol. **17:** 1827–1836.

Wang, G.-F., Ji, J., El-Kasmi, F., Dangl, J.L., Johal, G., and Balint-Kurti, P.J. (2015). Molecular and functional analyses of a maize autoactive NB-LRR protein identify precise structural requirements for activity. PLoS Pathog. **11:** e1004674.

Wormit, A., Butt, S.M., Chairam, I., McKenna, J.F., Nunes-Nesi, A., Kjaer, L., O'Donnelly, K., Fernie, A.R., Woscholski, R., Barter, M.C.L., and Hamann, T. (2012). Osmosensitive changes of carbohydrate metabolism in response to cellulose biosynthesis inhibition. Plant Physiol. **159:** 105–117.

Wu, G., and Poethig, R.S. (2006). Temporal regulation of shoot development in *Arabidopsis* thaliana by *miR156* and its target *SPL3.* Development **133:** 3539–3547.

Yamanaka, T., Nakagawa, Y., Mori, K., Nakano, M., Imamura, T., Kataoka, H., Terashima, A., Iida, K., Kojima, I., Katagiri, T., Shinozaki, K., and Iida, H. (2010). MCA1 and MCA2 that mediate Ca^{2+} uptake have distinct and overlapping roles in Arabidopsis. Plant Physiol. **152:** 1284–1296.

Yoshikawa, T., Eiguchi, M., Hibara, K., Ito, J., and Nagato, Y. (2013). Rice *slender leaf 1* gene encodes cellulose synthase-like D4 and is specifically expressed in M-phase cells to regulate cell proliferation. J. Exp. Bot. **64:** 2049–2061.

Zhang, L., Du, L., Shen, C., Yang, Y., and Poovaiah, B.W. (2014). Regulation of plant immunity through ubiquitin-mediated modulation of Ca^{2+}-calmodulin-AtSR1/CAMTA3 signaling. Plant J. **78:** 269–281.